Supporting information

Engineering a full gamut of structural colors in all-dielectric mesoporous network metamaterials

Alejandra Ruiz-Clavijo[1], Yoichiro Tsurimaki[2], Olga Caballero-Calero[1], George Ni[2], Gang Chen[2], Svetlana V. Boriskina[2]*, Marisol Martín-González[1,2]*

[1] IMN-Instituto de Micro y Nanotecnología (CNM-CSIC), Isaac Newton 8, PTM, E-28760 Tres Cantos, Madrid, Spain.
[2] Department of Mechanical Engineering, Massachusetts Institute of Technology, Cambridge, MA 02139, USA

*Corresponding authors: sborisk@mit.edu, marisol@imm.cnm.csic.es

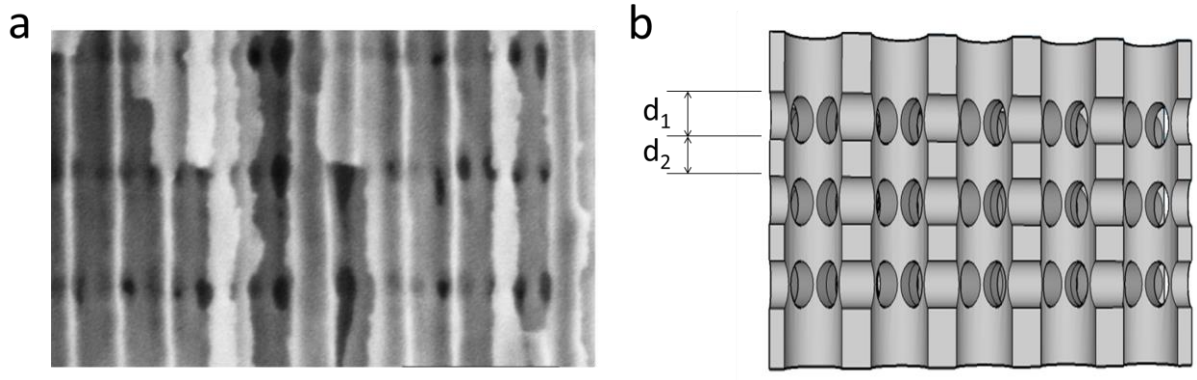

Supplementary Fig. S1. Cross view image (a) and schematic illustration (b) of a three-dimensional alumina membrane (3DAAO), where the high porosity layer with thickness d_1 and low porosity layer with thickness d_1 are defined.

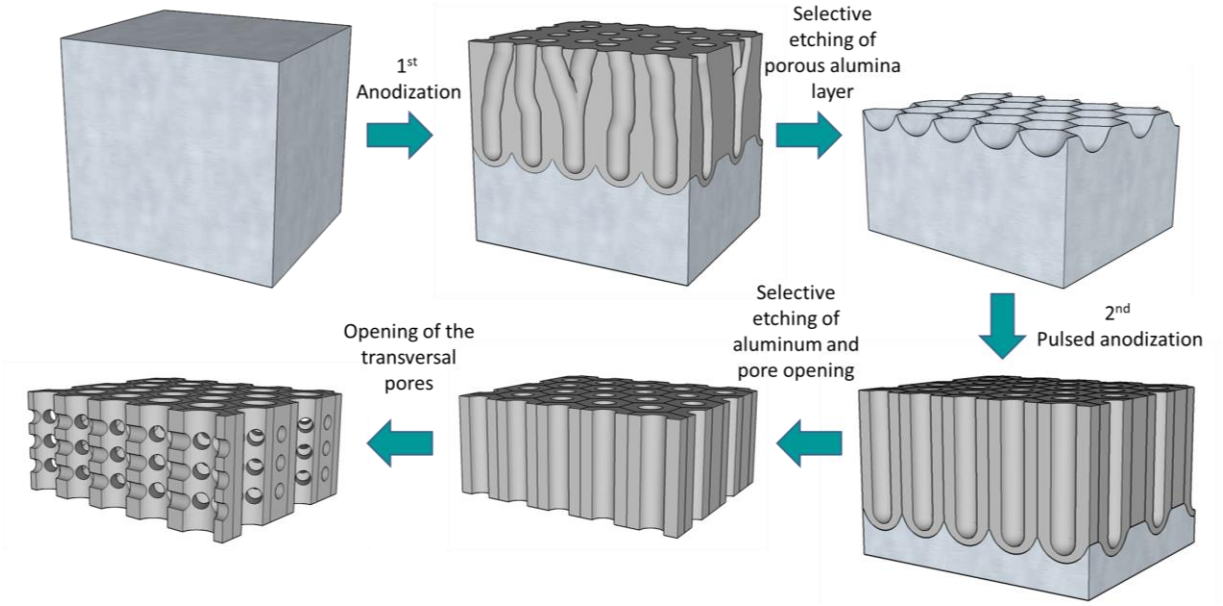

Supplementary Fig. S2. Schematic of the fabrication method used in the preparation of the 3D AAO porous metamaterial samples: Starting from pure aluminum (up-left), a first anodization is carried out, forming inhomogeneous pores at the surface, which get arranged in a hexagonal packaging after a certain anodization time (at a certain depth). Next, the alumina is removed by chemical etching, leaving an ordered patterned surface in the aluminum (up-right). Then, the second anodization is made, creating ordered pores. After the remaining aluminum and barrier layer removal (down-center image), the whole structure is immersed in phosphoric acid to reveal the transversal pores, created at the parts where the high voltages were applied in the second anodization step.

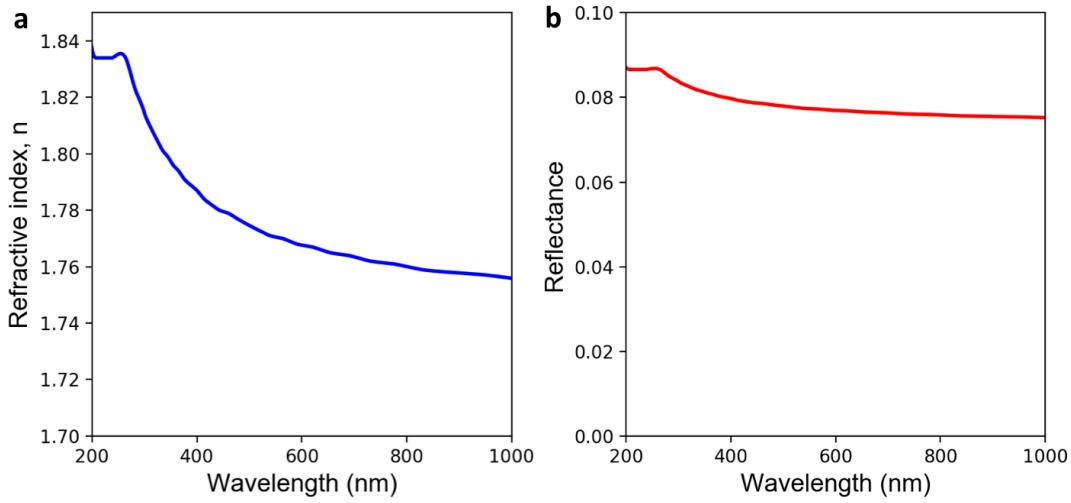

Supplementary Fig. S3. Refractive index (a) and reflectance (b) for normal incidence of bulk alumina (Al_2O_3) [1].

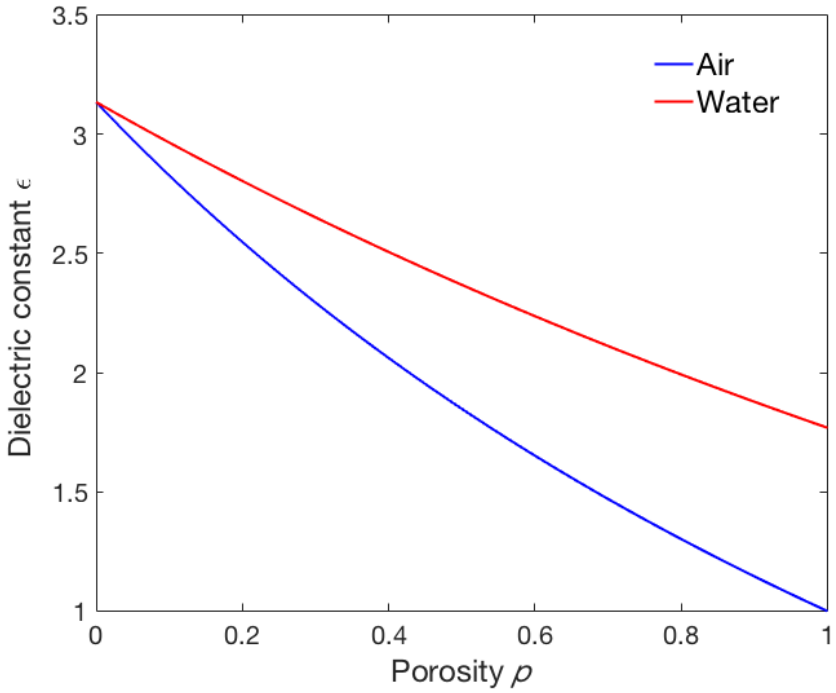

Supplementary Fig. S4. The effective dielectric constant of porous alumina calculated at a wavelength of 550nm via Maxwell-Garnett method as a function of material porosity. Two cases are considered: pores filled with air (blue line) and pores filled with water (red line). The dielectric constant of bulk Al_2O_3 at this frequency is 3.1329 (n=1.77, see also Fig. S3), and the dielectric constant of water is 1.777 (n=1.333).

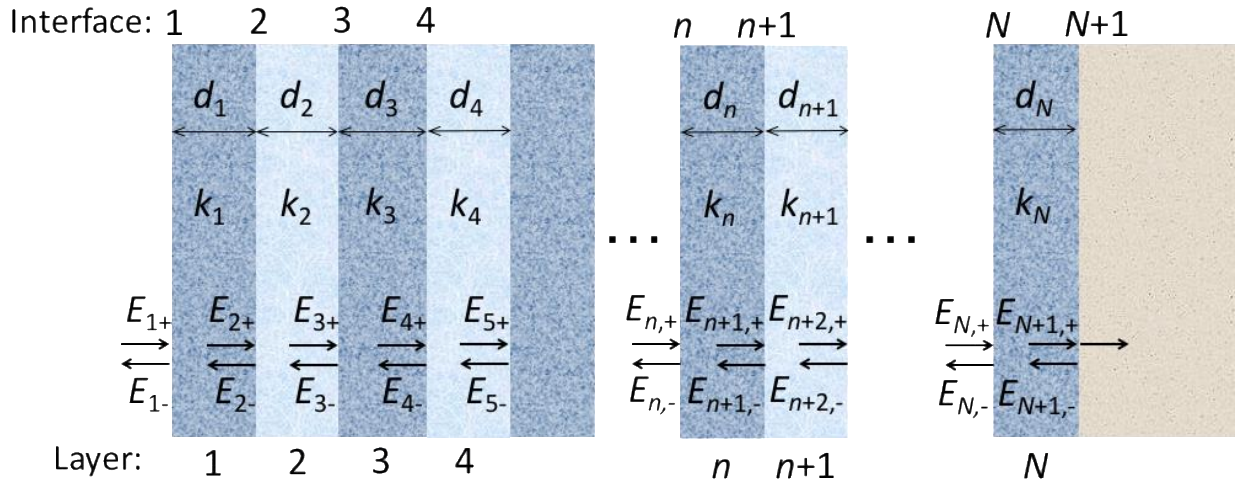

Supplementary Fig. S5. Schematic of the modeled multilayer structure with numbering convention of interfaces, layer parameters, as well as the strengths of the incident and reflected electric fields at each interface used in the Transfer Matrix Method calculations (see Methods).

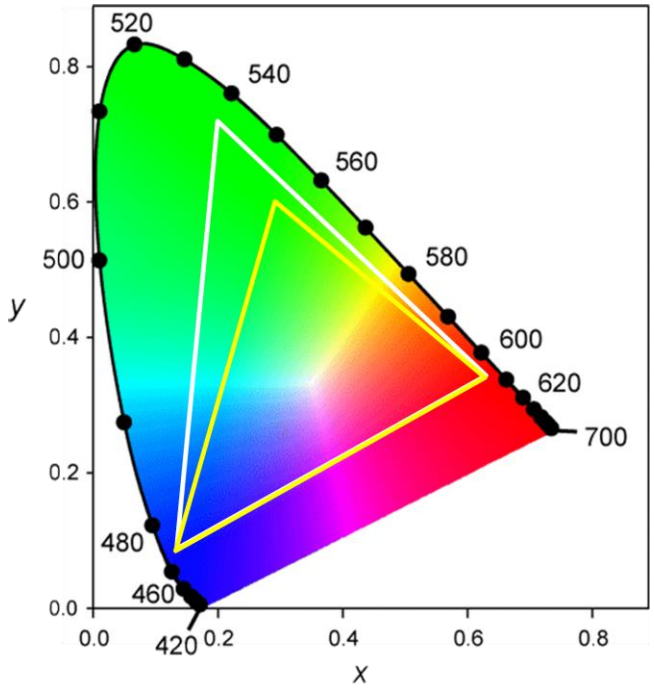

Supplementary Fig. S6. The CIE 1931 color space chromaticity diagram. The outer curved boundary is the spectral (or monochromatic) locus, with wavelengths shown in nanometers (image credit: Wikipedia). The CIE system characterizes colors by two-color coordinates X and Y, which correspond to a point on the chromaticity diagram. These coordinates are determined by the spectral power distribution of either emitted or reflected light and by the average sensitivity curves measured for the human eye (see Methods). The areas of the triangles illustrate the partial gamut of colors that can be matched by various combinations of red, green, and blue (RGB) in the color monitors. The yellow triangle covers the standard RGB (sRGB) gamut of colors represented in typical HDTV screens[2], and the white triangle covers the range of colors included in the Adobe RGB color space[3].

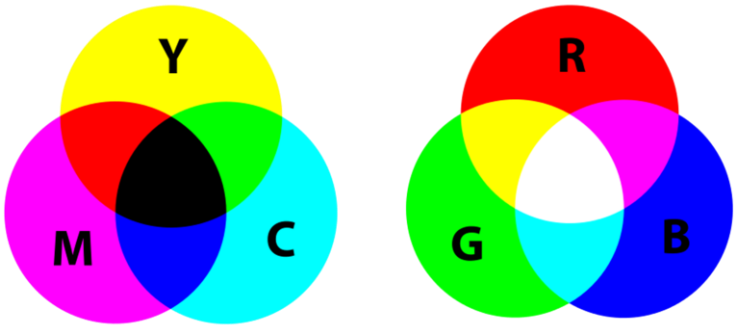

Supplementary Fig. S7. Pigment or additive (left) and structural or subtractive (right) color mixing diagrams. The sum of primary pigment colors yields black, while the addition of structural reflectance-based colors yields white (image credit: Wikipedia).

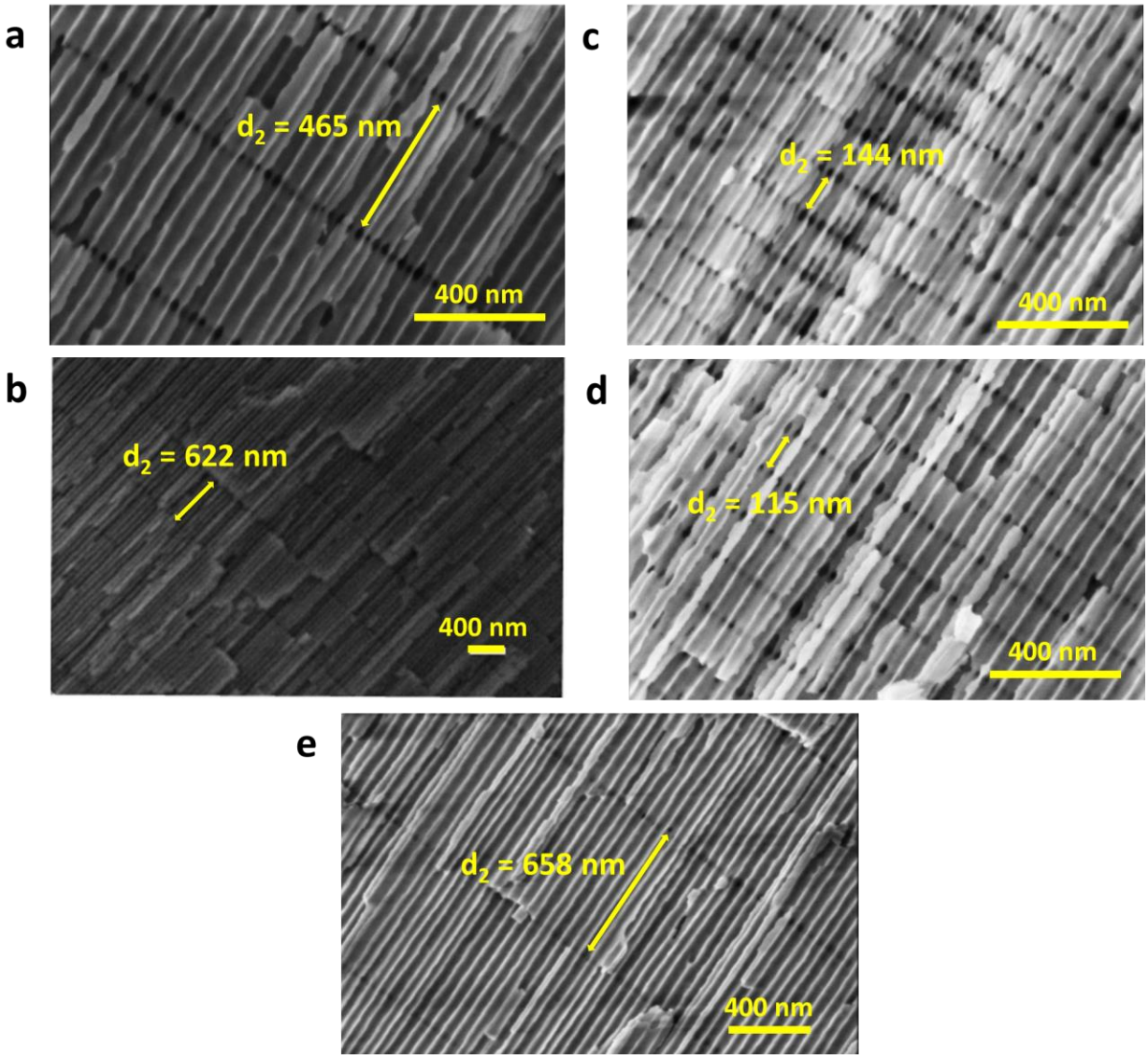

Supplementary Fig. S8. Scanning electron microscope images of the structure of the fabricated samples shown in Table 2: a) AAO3D1, b) AAO3D2, c) AAO3D3, d) AAO3D4, and e) AAO3D5.

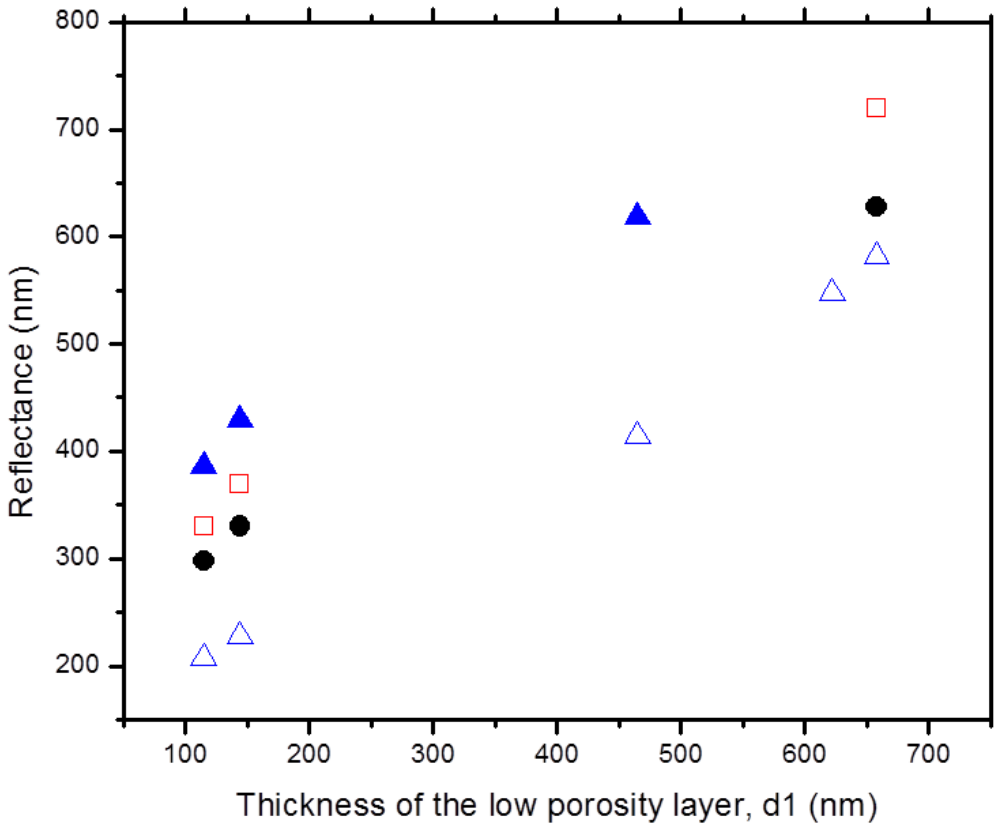

Supplementary Fig. S9. Shows the wavelength at which the maximum reflectance of the longest-wavelength peak contributing to the structural color formation (i.e., the rightmost peak in the visible reflectivity spectra) appears in the samples of Table 2 as a function of the sample's periodicity for the different incidence angles measured, 60° (solid black circles), 45° (open red squares), and 8° (solid blue triangles), to the normal. The open triangles represent the wavelength at which the next-order peak of the reflectivity spectra appears at an incident light of 8° from the normal. Note that for the thickest low porosity layer, the low-order reflectance peaks lie in the infrared, and thus are not shown, given that they are out of the detector range.

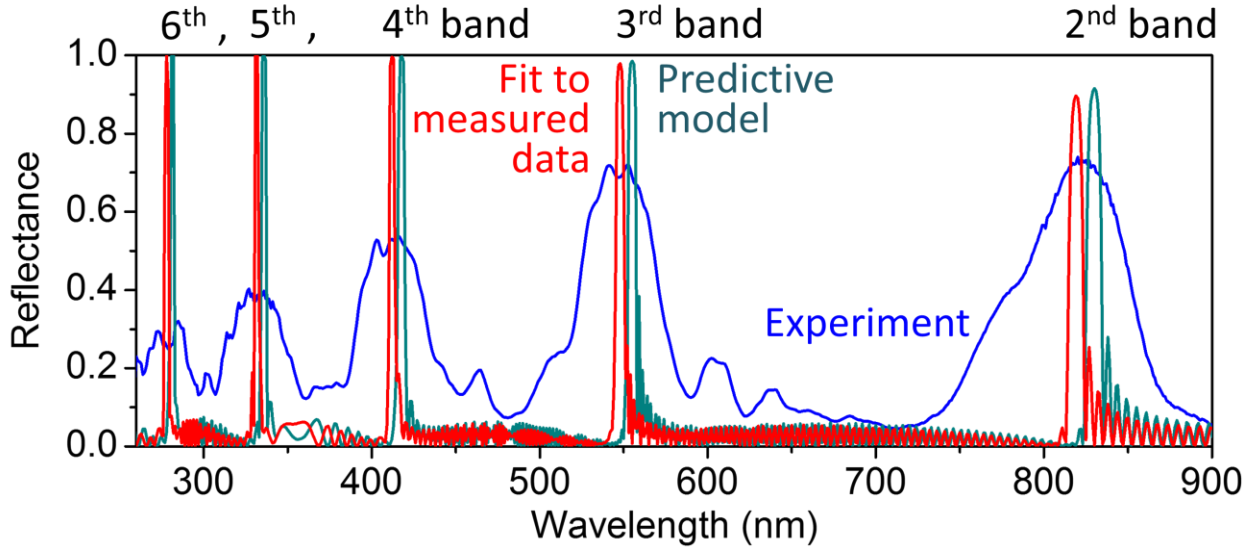

Supplementary Fig. S10. The reflectance spectrum of sample AAO3D2 across the ultra-violet, visible, and near-infrared parts of the electromagnetic spectrum. The teal line corresponds to the pre-fabrication model predictions for the sample with d_1=30nm, d_2=625nm, and porosities of 80% and 65%, respectively. The blue line is the experimentally measured spectrum. The red line is the best numerical fit to the experimental spectra, calculated for the structure with d_1=32nm, d_2=622nm (measured), and porosities of 80% and 67% (fitted). Experimental higher-order peaks get progressively more deformed and reduced in the magnitude due to fabrication imperfections.

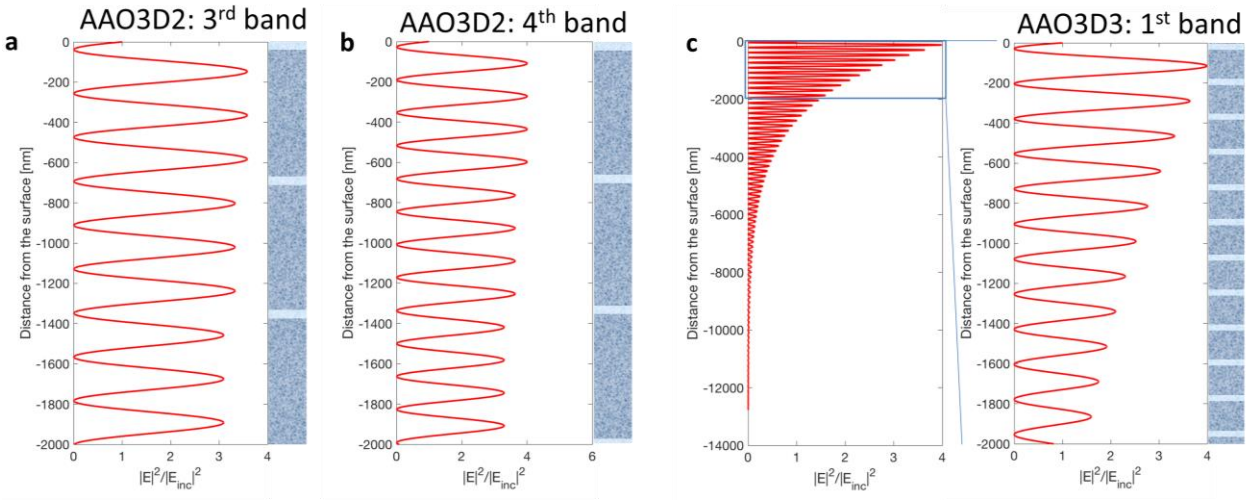

Supplementary Fig. S11. (a,b) The electric field distributions in the sample AAO3D2 at wavelengths 555 nm (a) and 418 nm (b), corresponding to the third and fourth stop bands of the porous metamaterial stack. The geometry of the multi-layered metamaterial stack is schematically shown to the right of each plot. The internal field variations within each layer are on the scale smaller than the pore sizes. This results in the spectral broadening of these bands and their deviation from the theoretical predictions made under the assumption of uniform layers with effective permittivity values. (c) The electric field

distribution in the sample AAO3D3 at wavelength 441 nm, corresponding to the first-order stop bands of this sample is shown for comparison. Comparison of panels (a,b) and (c) reveals deeper penetration lengths of the electric field into the sample at frequencies corresponding to the higher-order bands. This, in combination with multiple field variations within each low-porosity layer, makes high-order bands more sensitive to the fabrication details, including pore presence, pore non-uniformity, variations in the layer thickness, etc.

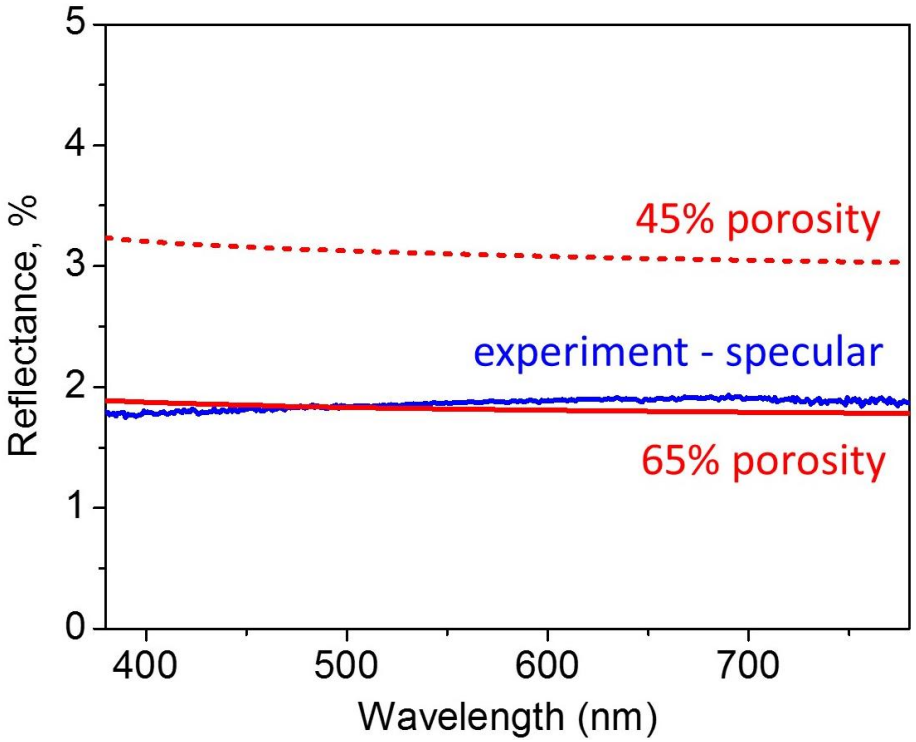

Supplementary Fig. S12. Reflectance spectra of a AAO sample without transverse pores. The incident angle is 8° from the normal. Blue: experimentally measured specular reflection spectrum. Solid red: calculated spectrum of a sample with 65% uniform porosity. Dashed red: calculated spectrum with 45% porosity value.

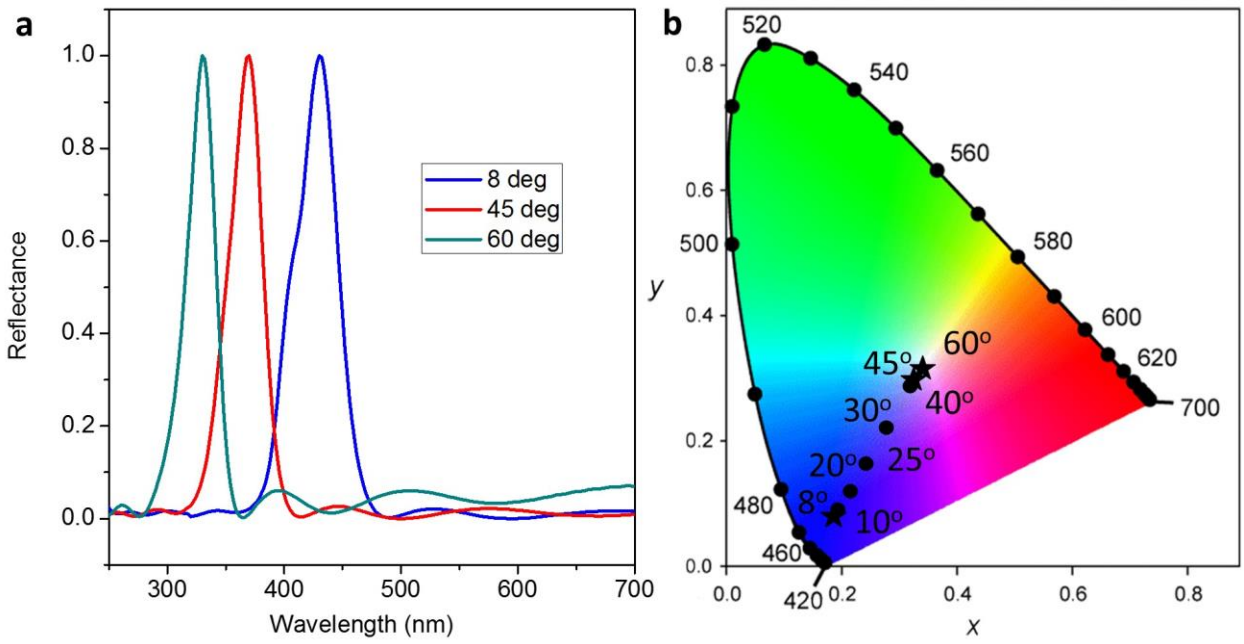

Supplementary Fig. S13. (a) Experimental reflectance spectra of sample AAO3D3 measured at 8° (blue), 45° (red), and 60° (teal) to the normal. (b) The points on the CIE chromaticity diagram corresponding to the experimental (stars) and calculated (dots) reflectance spectra at different angles measured from normal. The points move towards the center of the diagram with the increased angle of observation, resulting in the colorimetric response of the sample weakening and eventually dissapering at an angle of about 40°.

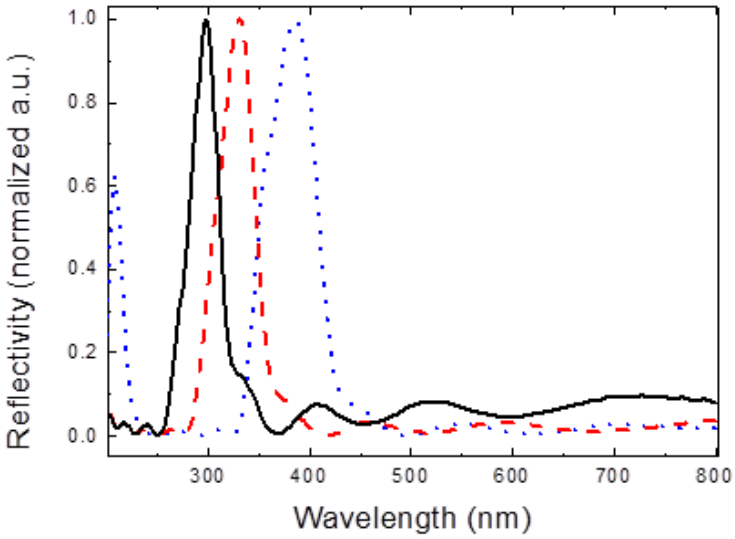

Supplementary Fig. S14. Experimental reflectance spectra of sample AAO3D4 measured at 8° (dotted blue), 45° (dashed red), and 60° (solid black) to the normal.

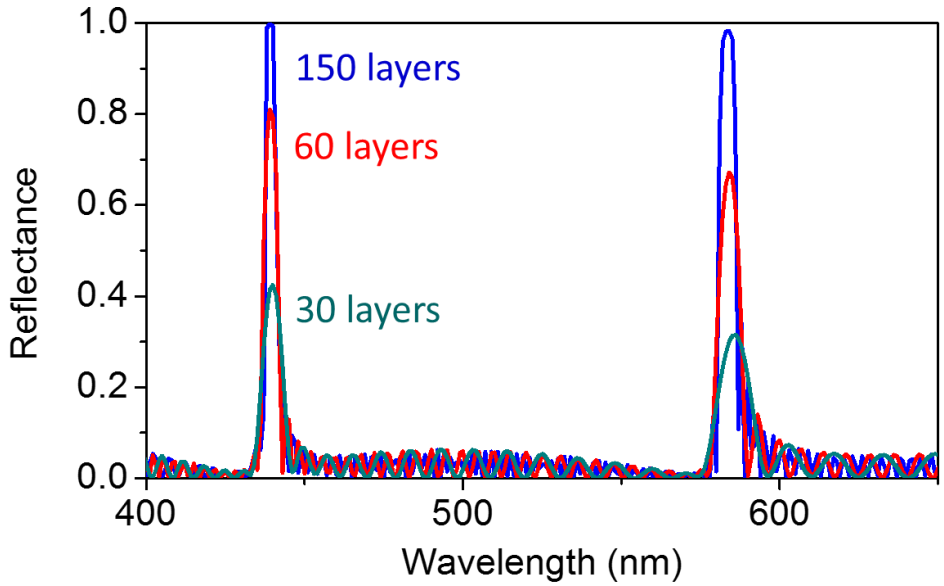

Supplementary Fig. S15. Calculated reflectance spectra for sample AAO3D5 obtained by using an increasing number of layers *N* (as labeled on the plot). Typical for the Bragg interference mechanism in periodic solids, the reflectance bands become more pronounced with the increase of the structure thickness, while their spectral positions remain virtually unchanged.

Supplementary video V1 shows the effect of wetting on the color change in sample A5.

References

1. E. D. Palik, *Handbook of Optical Constants of Solids* (Elsevier, 1997).

2. IEC 61966-2-1:1999. *IEC Webstore*. International Electrotechnical Commission.

3. "*Adobe RGB (1998) Color Image Encoding*," (Technical report). Adobe Systems Incorporated, 2005